

1           **A mechanistic model of an upper bound on oceanic carbon export as a**  
2           **function of mixed layer depth and temperature**

3   Zuchuan Li\*, Nicolas Cassar

4   Division of Earth and Ocean Sciences, Nicholas School of the Environment, Duke University,  
5   Durham, North Carolina, USA

6  
7   \* Corresponding author: Zuchuan Li ([zuchuan.li@duke.edu](mailto:zuchuan.li@duke.edu))

8  
9  
10 **Key points**

11   1. A mechanistic model of an upper bound on carbon export is developed based on the metabolic  
12   balance of photosynthesis and respiration in the oceanic mixed layer

13   2. Using parameters available in the literature, the modeled upper bound envelopes field  
14   observations of export production estimated from <sup>234</sup>Th and sediment traps and O<sub>2</sub>/Ar-derived net  
15   community production

16   3. The model identifies regions of the Southern Ocean where carbon export is likely limited by  
17   light during part of the growing season

21 **Abstract**

22 Export production reflects the amount of organic matter transferred from the surface ocean to depth  
23 through biological processes. This export is in great part controlled by nutrient and light  
24 availability, which are conditioned by mixed layer depth (MLD). In this study, building on  
25 Sverdrup's critical depth hypothesis, we derive a mechanistic model of an upper bound on carbon  
26 export based on the metabolic balance between photosynthesis and respiration as a function of  
27 MLD and temperature. We find that the upper bound is a positively skewed bell-shaped function  
28 of MLD. Specifically, the upper bound increases with deepening mixed layers down to a critical  
29 depth, beyond which a long tail of decreasing carbon export is associated with increasing  
30 heterotrophic activity and decreasing light availability. We also show that in cold regions the upper  
31 bound on carbon export decreases with increasing temperature when mixed layers are deep, but  
32 increases with temperature when mixed layers are shallow. A metaanalysis shows that our model  
33 envelopes field estimates of carbon export from the mixed layer. When compared to satellite export  
34 production estimates, our model indicates that export production in some regions of the Southern  
35 Ocean, most particularly the Subantarctic Zone, is likely limited by light for a significant portion  
36 of the growing season.

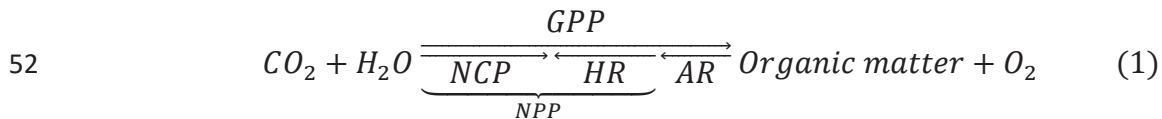
37 **Key words:** Export production, net community production, upper bound, mixed layer depth,  
38 temperature

39

40 **1. Introduction**

41 Photosynthesis in excess of respiration at the ocean surface leads to the production of organic  
42 matter, part of which is transported to the deep ocean through sinking and mixing (Volk and  
43 Hoffert, 1985). This biological process, known as export production (aka soft tissue biological  
44 carbon pump) lowers carbon dioxide (CO<sub>2</sub>) concentrations at the ocean surface and facilitates the  
45 flux of CO<sub>2</sub> from the atmosphere into the ocean (Falkowski et al., 1998; Ito and Follows, 2005;  
46 Sigman and Boyle, 2000).

47 Export production is frequently assumed to be a function of net community production (NCP)  
48 which is defined as the balance between net primary production (NPP) and heterotrophic  
49 respiration (HR), or the difference between gross primary production (GPP) and community  
50 respiration (CR; HR plus autotrophic respiration (AR)) (the acronyms used in this study are  
51 presented in Table 1) (Li and Cassar, 2016):



53 
$$Export\ production = NCP - MLD \times \frac{d(POC + DOC)}{dt} \quad (2)$$

54 where POC, DOC and MLD represent particulate organic carbon, dissolved organic carbon and  
55 mixed layer depth, respectively. If the organic carbon inventory (POC+DOC) in the mixed layer  
56 is at steady state, NCP is equal to export production (equation (2)). Without allochthonous sources  
57 of organic matter, if the organic matter inventory in the mixed layer decreases, NCP will be  
58 predicted to be transiently smaller than export production. Conversely, export may lag NPP  
59 (Henson et al., 2015; Stange et al., 2017), in which case NCP is expected to be greater than export  
60 production.

61 Net community production is in great part regulated by the availability of nutrients and light.  
62 Light availability exponentially decays with depth due to absorption by water and its constituents.  
63 The mixing of phytoplankton to depth therefore impacts phytoplankton physiology and  
64 productivity (Cullen and Lewis, 1988; Lewis et al., 1984), with the depth-integrated NPP expected  
65 to increase down to the euphotic depth. Respiration, on the other hand, is often modeled to be some  
66 function of organic matter concentration, which is expected to be constant with depth if  
67 homogeneously mixed within the mixed layer. Temperature is also believed to be an important  
68 control on carbon export because respiration is more temperature-sensitive than photosynthesis  
69 (Laws et al., 2000; López-Urrutia et al., 2006; Rivkin and Legendre, 2001). Field observations  
70 confirm that NCP is generally lower at high temperatures and consistently low when mixed layers  
71 are deep. These patterns have been attributed to the balance between depth-integrated  
72 photosynthesis (controlled by the availability of nutrients and light) and respiration as a function  
73 of MLD and temperature (Cassar et al., 2011; Eveleth et al., 2016; Huang et al., 2012; Shadwick  
74 et al., 2015; Tortell et al., 2015). However, descriptions of the underlying mechanisms heretofore  
75 remain qualitative. Likewise, the effects of light and nutrient on carbon fluxes are difficult to  
76 disentangle. For example, high-nutrient, low-chlorophyll regimes in the Southern Ocean have been  
77 attributed to iron limitation (Boyd et al., 2000), deep mixed layers and light limitation (Nelson and  
78 Smith, 1991; Mitchell and Holm-Hanse, 1991; Mitchell et al., 1991), or both (Sunda and Huntsman,  
79 1997). To decompose the influence of light and nutrient availability on NCP, we define the upper  
80 bound on carbon export from the mixed layer ( $NCP^*$ ) as the maximum export achievable should  
81 all limiting factors other than light (taking into account self-shading) be alleviated.

82 In his seminal paper, Sverdrup presented an elegant model to demonstrate that vernal  
83 phytoplankton blooms (i.e., organic matter accumulation at the ocean surface) may be driven by

84 increased light availability when the MLD shoals above a critical depth ( $Z_c$ ) (Sverdrup, 1953). In  
85 our study, we build upon Sverdrup (1953) and derive a mechanistic model of an upper bound on  
86 carbon export based on the metabolic balance of photosynthesis and respiration in the oceanic  
87 mixed layer, where the metabolic balance is derived from MLD, temperature, photosynthetically  
88 active radiation (PAR), phytoplankton maximum growth rate ( $\mu_{max}$ ), and heterotrophic activity.  
89 Our approach is analogous to other efforts where mechanistic models were derived to predict  
90 proxies of carbon export (e.g., Dunne et al. (2005) and Cael and Follows (2016)). We compare our  
91 *NCP\** model to observations, and use this model in conjunction with satellite export production  
92 estimates to identify regions in the world's oceans where light may limit export production. Our  
93 key findings are that 1) using parameters available in the literature, the modeled upper bound  
94 envelopes field observations of export production estimated from  $^{234}\text{Th}$  and sediment traps and  
95  $\text{O}_2/\text{Ar}$ -derived NCP, and 2) the model identifies regions of the Southern Ocean where carbon  
96 export is likely limited by light during part of the growing season.

## 97 **2. Model description and comparison to observations**

### 98 **2.1. Net community production and light availability**

99 A conceptual representation of the metabolic balance between volumetric NCP, NPP, and HR  
100 profiles is presented in Figure 1(A). According to equation (1), the volumetric NCP flux at a given  
101 depth ( $z$ ) in the mixed layer results from the difference between volumetric NPP and HR:

$$102 \quad NCP(z) = NPP(z) - HR(z) \quad (3)$$

103 where  $z$  increases with depth.  $NPP(z)$  is a function of the autotroph's intrinsic growth rate  
104 ( $\mu$ ) times their biomass concentration ( $C$ ). Assuming that the effect of nutrients and light on  
105 photosynthetic rates abides by Michaelis-Menten kinetics, and neglecting the effect of

106 photoinhibition (Dutkiewicz et al., 2001; Huisman and Weissing, 1994),  $NPP(z)$  may be  
 107 expressed as follows:

$$108 \quad NPP(z) = \mu(z) \times C = \frac{N}{N + k_m^N} \times \frac{I(z)}{I(z) + k_m^I} \times \mu_{max} \times C \quad (4)$$

109 where  $\mu_{max}$  is the maximum intrinsic growth rate of the autotrophic community;  $N$  and  $k_m^N$   
 110 represent the nutrient concentration and half-saturation constant, respectively; and  $I$  and  $k_m^I$   
 111 represent the irradiance level and half-saturation constant, respectively.  $\mu_{max}$ ,  $N$ ,  $k_m^N$ ,  $k_m^I$  and  $C$   
 112 are assumed to be well mixed within the mixed layer. The first two terms on the right-hand side of  
 113 equation (4) account for the effect of nutrient and light availability on autotrophic growth rates,  
 114 and they are hereafter defined as follows for simplicity:

$$115 \quad N_m = \frac{N}{N + k_m^N} \quad (5a)$$

$$116 \quad I_m(z) = \frac{I(z)}{I(z) + k_m^I} \quad (5b)$$

117  $I(z)$  is modeled as an exponential decay of PAR just beneath the water surface ( $I_0$ ):

$$118 \quad I(z) = I_0 \times e^{-K_I \times z} \quad (6)$$

119 where  $K_I$  is light attenuation coefficient which is assumed to be independent of depth in the mixed  
 120 layer.

121 As a first approximation, we assume that  $HR(z)$  is proportional to  $C$  as in previous studies  
 122 (Dutkiewicz et al., 2001; Huisman and Weissing, 1994; Rivkin and Legendre, 2001; Sverdrup,  
 123 1953; White et al., 1991):

$$124 \quad HR(z) = r_{HR} \times C \quad (7)$$

125 where  $r_{HR}$  represents the intrinsic heterotrophic respiration rate which is assumed to be dependent  
 126 on temperature (see below), and independent of depth. In reality,  $HR(z)$  is likely best modeled as

127 a function of the concentration of labile organic matter — an additional term could be included to  
 128 account for the relationship of total labile organic matter to  $C$ .

129 NCP integrated over the mixed layer ( $NCP(0, MLD)$ ) can be derived from equations (3-7):

$$\begin{aligned}
 130 \quad NCP(0, MLD) &= NPP(0, MLD) - HR(0, MLD) \\
 131 \quad &= \int_0^{MLD} NPP(z) dz - \int_0^{MLD} HR(z) dz \\
 132 \quad &= N_m \times I_m(0, MLD) \times \mu_{max} \times C - r_{HR} \times MLD \times C \quad (8)
 \end{aligned}$$

133 The first term on the right side of equation (8) represents NPP integrated over the mixed layer  
 134 ( $NPP(0, MLD)$ ), which is equivalent to the product of  $\int_0^{MLD} \mu(z) dz$  and  $C$ , where the former term  
 135 is modeled to be a function of  $\mu_{max}$  conditioned by nutrient and light availability within the mixed  
 136 layer.  $I_m(0, MLD)$  can be derived as follows:

$$137 \quad I_m(0, MLD) = \int_0^{MLD} I_m(z) dz = -\frac{1}{K_I} \times \ln \left( \frac{I_0 \times e^{-K_I \times MLD} + k_m^I}{I_0 + k_m^I} \right) \quad (9)$$

138 NCP integrated over the mixed layer (equation (8)) is a bell-shaped function of MLD as depicted  
 139 in the schematic diagram of Figure 1(B).

## 140 **2.2. Net community production and phytoplankton biomass concentration**

141 As can be seen from equation (8),  $NCP(0, MLD)$  is a direct function of  $C$  because  
 142  $NPP(0, MLD)$  and  $HR(0, MLD)$  are proportional to  $C$ .  $NCP(0, MLD)$  is also an indirect function  
 143 of  $C$  due its effect on light attenuation (i.e.,  $K_I$ ). The attenuation coefficient  $K_I$  can be divided into  
 144 water and non-water components ( $K_I = K_I^w + K_I^{nw}$ ) (Baker and Smith, 1982; Smith and Baker,  
 145 1978a; Smith and Baker, 1978b), where  $K_I^{nw}$  is controlled by the concentrations of phytoplankton,  
 146 colored dissolved organic matter (CDOM), and non-algal particles (NAP). In the open ocean where  
 147 CDOM and NAP co-vary with phytoplankton (Morel and Prieur, 1977),  $K_I$  can be related to  $C$  as  
 148 follows:

149 
$$K_I = K_I^w + k_c \times C \quad (10)$$

150 where  $k_c$  is a function of the solar zenith angle, the specific absorption and backscattering  
 151 coefficients of phytoplankton, and the relationship between phytoplankton, CDOM, and NAP.  
 152 Because pure water and phytoplankton attenuate light,  $K_I^w$  and  $k_c$  should be greater than zero.

153 To calculate how  $NCP(0, MLD)$  varies as a function of  $C$ , we examine its first  $(\frac{dNCP(0, MLD)}{dC})$   
 154 and second  $(\frac{d^2NCP(0, MLD)}{dC^2})$  derivatives with respect to  $C$  based on equations (8) and (10):

155 
$$\frac{dNCP(0, MLD)}{dC}$$
  
 156 
$$= N_m \times \mu_{max} \times \frac{K_I^w \times I_m(0, MLD) + k_c \times C \times MLD \times I_m(MLD)}{K_I^w + k_c \times C} - r_{HR} \times MLD \quad (11)$$

157 
$$\frac{d^2NCP(0, MLD)}{dC^2} = N_m \times k_c \times \frac{\mu_{max}}{K_I}$$
  
 158 
$$\times \left\{ \frac{2 \times K_I^w}{K_I} \times (MLD \times I_m(MLD) - I_m(0, MLD)) - \frac{k_c \times C \times I_m(MLD)^2 \times MLD^2 \times k_m^I}{I_0 \times e^{-K_I \times MLD}} \right\} \quad (12)$$

159 when  $MLD > 0$ ,  $I_m(0, MLD) > MLD \times I_m(MLD)$ :

160 
$$I_m(0, MLD) = \int_0^{MLD} \frac{I_0 \times e^{-K_I \times z}}{I_0 \times e^{-K_I \times z} + k_m^I} dz$$
  
 161 
$$> \int_0^{MLD} \frac{I_0 \times e^{-K_I \times MLD}}{I_0 \times e^{-K_I \times MLD} + k_m^I} dz = MLD \times I_m(MLD) \quad (13)$$

162 The detailed derivation of equations (11-12) can be found in the supplementary material.

163 Substituting the inequality (13) into equation (12) gives  $\frac{d^2NCP(0, MLD)}{dC^2} < 0$ , which suggests that

164  $\frac{dNCP(0, MLD)}{dC}$  decreases with increasing  $C$ . Because increasing  $C$  decreases light availability due to

165 shelf-shading,  $NPP(0, MLD)$  saturates with increasing  $C$ . Thus,  $NCP(0, MLD)$  will reach an

166 asymptote of  $\lim_{C \rightarrow \infty} (\frac{dNCP(0, MLD)}{dC}) = -r_{HR} \times MLD < 0$ , because  $HR(0, MLD)$  linearly increases



167 with increasing  $C$  while  $NPP(0, MLD)$  plateaus (Figure 2). Additionally, because  $NCP(0, MLD)$   
 168 must be nil when there is no autotrophic biomass ( $NCP(0, MLD)|_{C=0} = 0$ ),  $\lim_{C \rightarrow 0} \left( \frac{dNCP(0, MLD)}{dC} \right)$  must  
 169 be greater than zero, otherwise the ecosystem would be net heterotrophic which is unachievable  
 170 without an allochthonous source of organic matter.  $\lim_{C \rightarrow 0} \left( \frac{dNCP(0, MLD)}{dC} \right) > 0$  and  $\lim_{C \rightarrow \infty} \left( \frac{dNCP(0, MLD)}{dC} \right) =$   
 171  $-r_{HR} \times MLD < 0$  suggest the existence of  $\left. \frac{dNCP(0, MLD)}{dC} \right|_{C=C^*} = 0$  where  $C^*$  corresponds to an  
 172 autotrophic biomass concentration which maximizes  $NCP(0, MLD)$  (i.e.,  $NCP^*$ ).

173 The dependence of  $NCP(0, MLD)$  on  $C$  can be conceptually understood in the following way.  
 174 Given a water column with sufficient nutrients, the critical depth  $Z_c$  and compensation depth  $Z_p$   
 175 are expected to shoal as  $C$  increases. When  $C$  is low,  $NCP(0, MLD)$  increases with  $C$  because of  
 176 its greater impact on  $NPP(0, MLD)$  than on  $HR(0, MLD)$ . As  $C$  further increases, the increase in  
 177  $NPP(0, MLD)$  with  $C$  slows because of light attenuation (i.e.,  $K_l$ ). There is therefore a  $C^*$  which  
 178 maximizes the difference between  $NPP(0, MLD)$  and  $HR(0, MLD)$  leading to  $NCP^*$  (Figure 2).  
 179 Beyond this point ( $C^*$ ), further increasing  $C$  will cause self-shading and limit photosynthesis in the  
 180 deep part of the mixed layer, as a result decreasing  $NCP(0, MLD)$ . Beyond a critical biomass ( $C_c$ ),  
 181 the ecosystem becomes net heterotrophic. Without an allochthonous source of organic carbon, this  
 182 is only transiently sustainable.

### 183 2.3. Mixed layer depth and compensation depth

184 By definition, if  $NCP(MLD)$  is smaller than zero (i.e., net heterotrophy at the bottom of the  
 185 mixed layer), the MLD must be deeper than  $Z_p$  ( $MLD > Z_p$ ) (and vice versa). To determine the  
 186 sign of  $NCP(MLD)$ , we substitute inequality (13) into equation (11). According to the inequality  
 187 presented in equation (13),  $\frac{K_l^w \times I_m(0, MLD) + k_c \times C \times MLD \times I_m(MLD)}{K_l^w + k_c \times C}$  in equation (11) must be greater than

188  $\frac{K_l^w \times MLD \times I_m(MLD) + k_c \times C \times MLD \times I_m(MLD)}{K_l^w + k_c \times C}$  (which is equal to  $MLD \times I_m(MLD)$ ). After simple

189 rearrangements, the substitution of inequality (13) into equation (11) leads to:

$$190 \quad \frac{dNCP(0, MLD)}{dC}$$

$$191 \quad > MLD \times (N_m \times I_m(MLD) \times \mu_{max} - r_{HR}) = \frac{MLD}{C} \times NCP(MLD) \quad (14)$$

192 The inequality in equation (14) in turn suggests that when  $NCP(0, MLD)$  is maximized

193 ( $\frac{dNCP(0, MLD)}{dC} = 0$ ),  $NCP(MLD)$  is negative (net heterotrophic) and hence the MLD is deeper than

194  $Z_p$  ( $MLD > Z_p$ ). This counterintuitive result is attributable both to the uneven distribution of light

195 availability in the water column (equation (13)) and to water which absorbs light but does not

196 contribute to biomass accumulation. When the mixed layer is at the  $Z_p$ , a slight increase in  $C$  will

197 leads to negative  $NCP(MLD)$  due to decreasing light availability at the base of mixed layer, but

198 will increase NCP higher in the water column because of the increase in biomass. The increase in

199 NCP in the shallow parts of the mixed layer therefore overcompensates for the net heterotrophy at

200 the bottom of the mixed layer, thus maximizing the depth-integrated NCP. If light were uniformly

201 distributed in the water column (i.e.,  $I_m(0, MLD) = MLD \times I_m(MLD)$ ) and if water did not

202 attenuate light ( $K_l^w = 0$  in equation (11)),  $MLD = Z_p$  would maximize  $NCP(0, MLD)$ , which is

203 consistent with Huisman and Weissing (1994). We note that in equation (14) the NCP profile

204 ( $NCP(z)$ ) varies with increasing  $C$ , which is different from what is conceptually presented in

205 Figure 1. The depth-integrated NCP in Figure 1 maximizes at the compensation depth because the

206 NCP profile ( $NCP(z)$ ) is assumed to be invariant.

#### 207 **2.4. An upper bound on carbon export**

208 Equations (11-13) delineate the conditions for an upper bound on carbon export ( $NCP^*$ ). In

209 order to simplify the relationship of  $NCP^*$  to MLD and temperature, we approximate  $I_m(0, MLD)$ :

210 
$$I_m(0, MLD) = -\frac{1}{K_I} \times \ln \left( 1 + \frac{I_0}{I_0 + k_m^I} \times (e^{-K_I \times MLD} - 1) \right)$$

211 
$$\approx -\frac{1}{K_I} \times \ln(1 - I_m(0)) \quad (15)$$

212 where  $I_m(0) = \frac{I_0}{I_0 + k_m^I}$ . Based on equation (15),  $NCP(0, MLD)$  in equation (8) can be approximated

213 as:

214 
$$NCP(0, MLD) = C \times MLD \times \left( \frac{1}{K_I \times MLD} \times \mu^* - r_{HR} \right) \quad (16)$$

215 where  $\mu^* = -\ln(1 - I_m(0)) \times N_m \times \mu_{max}$ . To evaluate the approximation accuracy of equation

216 (15), we compare the upper bounds estimated from equation (16) and the original model (equations

217 (8-10)). Our comparison suggests that the approximation of equation (15) is accurate for the

218 estimation of  $NCP^*$  under most conditions (Figure 3).

219 We first need to derive the  $C^*$  which maximizes  $NCP(0, MLD)$  (i.e.,  $NCP^*$ ) in equation (16).

220  $C^*$  can be solved from the first derivative of  $NCP(0, MLD)$  in equation (16) with respect to  $C$ :

221 
$$\left. \frac{dNCP(0, MLD)}{dC} \right|_{NCP(0, MLD)=NCP^*} = \mu^* \times \frac{K_I^W}{(k_c \times C^* + K_I^W)^2} - MLD \times r_{HR} = 0 \quad (17)$$

222

223 and therefore:

224 
$$C^* = \frac{1}{k_c} \times \left[ -K_I^W + \sqrt{\frac{\mu^* \times K_I^W}{MLD \times r_{HR}}} \right] \quad (18)$$

225 Equation (18) decreases with MLD. As  $C^*$  is positive ( $C^* \geq 0$ ) and cannot go to infinity ( $C^* \leq$

226  $C_{max}^*$ ), MLD should satisfy  $MLD_{C_{max}^*} \leq MLD \leq \frac{\mu^*}{r_{HR} \times K_I^W}$ , where  $MLD_{C_{max}^*}$  represents the MLD

227 corresponding to the maximum achievable autotroph's biomass concentration ( $C_{max}^*$ ) in the

228 surface ocean. The  $NCP^*$  model for  $0 \leq MLD < MLD_{C_{max}^*}$  is not discussed here, because we do

229 not have data with very shallow MLD to constrain and evaluate the model. The derivation of the  
 230 model is however presented in the supplementary material. Substituting  $C^*$  from equation (18) into  
 231 equation (16):

$$232 \quad \sqrt{NCP^*} = a_2 \times \sqrt{-\ln(1 - I_m(0))} + a_1 \times \sqrt{MLD} \quad (19)$$

233 where  $a_1 = -\sqrt{\frac{K_l^w \times r_{HR}}{k_c}}$  and  $a_2 = \sqrt{\frac{N_m \times \mu_{max}}{k_c}}$ . Constants  $a_1$  and  $a_2$  are functions of  $r_{HR}$  and  $\mu_{max}$ ,  
 234 respectively, which are generally modeled to increase with temperature ( $T$ ) (Eppley, 1972; Rivkin  
 235 and Legendre, 2001):

$$236 \quad \mu_{max} = \mu_{max}^0 \times e^{P_t \times T} \quad (20a)$$

$$237 \quad r_{HR} = r_{HR}^0 \times e^{B_t \times T} \quad (20b)$$

238 where  $P_t$  and  $B_t$  are constants; and  $\mu_{max}^0$  and  $r_{HR}^0$  are maximum growth rate and heterotrophic  
 239 respiration ratio for  $T = 0$  °C, respectively.  $P_t$  is commonly assumed to equal 0.0663 (Eppley,  
 240 1972). Substituting equations (20a) and (20b) into equation (19) yields:

$$241 \quad \sqrt{NCP^*} = a_4 \times \sqrt{e^{P_t \times T}} \times \sqrt{-\ln(1 - I_m(0))} + a_3 \times \sqrt{e^{B_t \times T}} \times \sqrt{MLD} \quad (21)$$

$$242 \quad \text{where } a_3 = -\sqrt{\frac{r_{HR}^0 \times K_l^w}{k_c}} \text{ and } a_4 = \sqrt{\frac{\mu_{max}^0 \times N_m}{k_c}}.$$

## 243 **2.5. Comparison to observations**

### 244 **2.5.1 Data products**

245 We assess the performance of our modeled upper bound on carbon export using a global dataset  
 246 of MLD, PAR, sea surface temperature (SST),  $O_2/Ar$ -derived NCP, and export production derived  
 247 from sediment traps and  $^{234}Th$  (see supplementary material). MLD was derived from global Argo  
 248 profiles (Global Ocean Data Assimilation Experiment; <http://www.usgodae.org/>) and CTD casts  
 249 (National Oceanographic Data Center; <https://www.nodc.noaa.gov/>). PAR was downloaded from

250 the NASA ocean color website (<https://oceancolor.gsfc.nasa.gov/>). The NCP estimates are based  
251 on a compilation of O<sub>2</sub>/Ar measurements from Li and Cassar (2016), Li et al. (2016), Shadwick et  
252 al. (2015), and Martin et al. (2013). The POC export production estimates were obtained from the  
253 recently compiled dataset of Mouw et al. (2016). These estimates were adjusted to reflect a flux at  
254 the base of mixed layer using the Martin curve of organic carbon attenuation with depth (Martin  
255 et al., 1987). The constants  $k_c$  and  $K_I^w$  in equation (10) were derived assuming a carbon to  
256 chlorophyll *a* ratio of 90 (Arrigo et al., 2008) and an empirical linear relationship between  $K_I$  and  
257 chlorophyll *a* concentration (see Figure S3), calculated based on the NOMAD dataset (Werdell  
258 and Bailey, 2005).  $k_m^I$  was set at 4.1 Einstein m<sup>-2</sup> d<sup>-1</sup> following Behrenfeld and Falkowski (1997).  
259 In our estimation of the upper bound on carbon export, we set  $N_m$  to 1 in the  $NCP^*$  calculations.

## 260 **2.5.2 Results and discussion**

261 Overall, we find that  $NCP^*$  calculated using published parameters (Table 2) does a good job  
262 of enveloping carbon export observations reported in the literature (Figure 4(A)). Samples on the  
263  $NCP^*$  envelope (upper bound) are likely regulated by light availability. Conversely, points below  
264 the upper bound may be nutrient limited. As expected,  $NCP^*$  increases with  $\mu_{max}$  and decreases  
265 with  $r_{HR}$ . Model parameters  $a_1 = -1.78$  and  $a_2 = 14.75$  (equation (19)) provide the best fit to the  
266 upper bound of O<sub>2</sub>/Ar-NCP as a function of MLD. When compared to parameters available in the  
267 literature (Table 2), we find that the best fit to our modeled upper bound is using  $\mu_{max}$  and  $r_{HR}$  of  
268 1.2 d<sup>-1</sup> and 0.2 d<sup>-1</sup>, respectively. When accounting for the effect of  $T$  on  $\mu_{max}$  and  $r_{HR}$ , model  
269 constants  $a_3 = -1.53$  and  $a_4 = 13.39$  (equation (21)) best fit the upper bound on O<sub>2</sub>/Ar-NCP,  
270 SST and MLD observations.

271 Our results show that  $NCP^*$  decreases faster with increasing MLD in warmer waters (Figures  
272 4(B) and 4(C)), because the term  $a_3 \times \sqrt{e^{Bt \times T}}$  in equation (21) is negative and negatively

273 correlated to  $T$ . This temperature effect contributes to part of the relationship between export  
 274 production and MLD in Figure 4(A). Interestingly,  $NCP^*$  increases with  $T$  in colder waters and  
 275 shallow mixed layers (Figure 4(C)). This is because  $NCP^*$  reflects the balance between  
 276 productivity ( $a_4 \times \sqrt{e^{P_t \times T}} \times \sqrt{-\ln(1 - I_m(0))}$ ) and heterotrophic respiration ( $a_3 \times \sqrt{e^{B_t \times T}} \times$   
 277  $\sqrt{MLD}$ ). In a shallow cold mixed layer, the change in productivity with  $T$   
 278 ( $\frac{d(a_4 \times \sqrt{e^{P_t \times T}} \times \sqrt{-\ln(1 - I_m(0))})}{dT} = \frac{P_t}{2} \times a_4 \times \sqrt{e^{P_t \times T}} \times \sqrt{-\ln(1 - I_m(0))}$ ) is greater than that of  
 279 heterotrophic respiration ( $\frac{d(a_3 \times \sqrt{e^{B_t \times T}} \times \sqrt{MLD})}{dT} = \frac{B_t}{2} \times a_3 \times \sqrt{e^{B_t \times T}} \times \sqrt{MLD}$ ). These results could  
 280 explain part of the variability in the relationship between NCP and SST reported in previous studies  
 281 (Li and Cassar, 2016). Our  $NCP^*$  model does not perform as well in warmer deep mixed layers,  
 282 where high variability in export ratio maxima have also been reported (Cael and Follows, 2016).  
 283 This may stem from uncertainties in observations, the differing relationship between  $T$ ,  $\mu_{max}$ , and  
 284  $r_{HR}$  at high temperature, and/or violations of our assumptions (see caveats and limitations).

285 Several recent studies have explored the relationship of NCP to oceanic parameters based on  
 286 various statistical approaches (Cassar et al., 2015; Chang et al., 2014; Huang et al., 2012; Li and  
 287 Cassar, 2016; Li et al., 2016). Our model can shed some light into the mechanisms driving some  
 288 of these patterns. To that end, we substitute equation (9) into equation (8):

$$289 \quad NCP(0, MLD) = C \times MLD \times \left( -\frac{N_m \times \mu_{max}}{K_I \times MLD} \times \ln \left( \frac{I_0 \times e^{-K_I \times MLD} + k_m^I}{I_0 + k_m^I} \right) - r_{HR} \right) \quad (22)$$

290 Rearranging equation (22):

$$291 \quad NCP_B = \frac{NCP(0, MLD)}{C \times MLD} = -\frac{\ln \left( \frac{I_0 \times e^{-K_I \times MLD} + k_m^I}{I_0 + k_m^I} \right)}{I_0 \times (1 - e^{-K_I \times MLD})} \times N_m \times \mu_{max} \times PAR_{ML} - r_{HR} \quad (23)$$

292 where  $NCP_B$  is the biomass-normalized volumetric NCP,  $PAR_{ML}$  is the average PAR in the mixed

293 layer ( $PAR_{ML} = \frac{1-e^{-K_I \times MLD}}{K_I \times MLD} \times I_0$ ), and  $-\frac{\ln\left(\frac{I_0 \times e^{-K_I \times MLD} + k_m^I}{I_0 + k_m^I}\right)}{I_0 \times (1-e^{-K_I \times MLD})} \times N_m \times \mu_{max}$  and  $-r_{HR}$  correspond

294 to the slope and offset, respectively. The scatter in the relationship between chlorophyll-

295 normalized volumetric NCP and  $PAR_{ML}$ , as reported in previous studies (Bender et al., 2016), can

296 likely be explained by the effect of temperature and the availability of nutrient and light (among

297 other properties) on the slope and offset of equation (23). Equation (22) can also be reorganized to

298 assess how environmental conditions may impact the export ratio ( $ef$ ):

$$299 \quad ef = \frac{NCP(0, MLD)}{NPP(0, MLD)} = 1 - \frac{K_I \times MLD}{-\ln\left(\frac{I_0 \times e^{-K_I \times MLD} + k_m^I}{I_0 + k_m^I}\right)} \times \frac{1}{N_m} \times \frac{r_{HR}}{\mu_{max}} \quad (24)$$

300 where  $\frac{r_{HR}}{\mu_{max}}$  is proportional to  $e^{(B_t - P_t) \times T}$ . Equation (24) is consistent with multiple studies which

301 predict decreasing  $ef$  with increasing temperature (Cael and Follows, 2016; Dunne et al., 2005;

302 Henson et al., 2011; Laws et al., 2000; Li and Cassar, 2016). In fact, equation (5) of Cael and

303 Follows (2016) can easily be derived from equation (24) (see supplementary material). Equation

304 (24) also highlights that a multitude of factors may confound the dependence of  $ef$  on temperature

305 (including varying MLD, light attenuation, and availability of nutrient and light). This again may

306 explain some of the conflicting observations recently reported in the literature (e.g., Maiti et al.

307 (2013)), where the effect of temperature may be masked by changes in community composition

308 (Britten et al., 2017; Henson et al., 2015). One therefore needs to account or correct for the

309 multitude of confounding factors when predicting the effect of a given environmental condition

310 (e.g., temperature, mineral ballast, and NPP) on the export ratio.

### 311 **3. Spatial distribution of the upper bound on carbon export**

312 We estimate the global distribution of the upper bound of carbon export using equation (19)  
313 and climatological monthly MLD and PAR. In general,  $NCP^*$  is high in low latitudes and low in  
314 the North Atlantic and Antarctic Circumpolar Current (ACC) in the Southern Ocean (Figure 5(A)).  
315 As expected, this spatial pattern is controlled by MLD (see Figure S1). Satellite-derived estimates  
316 of NCP (Li and Cassar, 2016) are approximately 10% of global  $NCP^*$ , reflecting the high degree  
317 of nutrient limitation in the oceans. We also derive a global  $NCP^*$  map using equation (21), and  
318 find that the global  $NCP^*$  estimate is very sensitive to the temperature dependence of  $r_{HR}$ . For  
319 example, decreasing the  $B_t$  in  $r_{HR} = r_{HR}^0 \times e^{B_t \times T}$  from 0.11 to 0.08 (as used in Rivkin and  
320 Legendre (2001) and López-Urrutia et al. (2006)) increases the global  $NCP^*$  budget by a factor of  
321 2.4. Large differences in  $NCP^*$  in low-latitudes in great part explain this change. In light of the  
322 large uncertainties in the relationship between  $r_{HR}$  and  $T$  (Cael and Follows, 2016; López-Urrutia  
323 et al., 2006), we hereafter only discuss  $NCP^*$  estimates derived from equation (19).

324 To estimate how close export production is to its upper bound, we calculate the ratio of export  
325 production to  $NCP^*$  ( $f_{pt}$ ). Low  $f_{pt}$  regimes represent ecosystems likely regulated by nutrient  
326 availability (i.e., ecosystems that have not reached their full export potential based on MLD and  
327 surface PAR). As expected, low latitude and subtropical regions have low  $f_{pt}$  (Figure 5(B)). High  
328  $f_{pt}$  regimes represent ecosystems which have reached their full light potential, and are therefore  
329 less likely to respond to nutrient addition because of light limitation (e.g., North Atlantic and ACC  
330 (Figure 5(B))). In these regions, especially the subantarctic region,  $f_{pt}$  is high in the spring (Figure  
331 5(C)) and decreases in the summer (Figure 5(D)), suggesting that export production is likely co-  
332 limited by nutrient and light availability. This may in part explain the lower response to iron  
333 fertilization in the subantarctic region where substantial increases in surface chlorophyll were only



334 observed in regions with shallower mixed layers (Boyd et al., 2007; Boyd et al., 2000; de Baar et  
335 al., 2005).

336 Also shown in Figure 5 are the biological pump efficiency and export ratio  $ef$  (panels 5E and  
337 5F, respectively). These various proxies reflect different components of the biological pump.  
338 Whereas  $f_{pt}$  reflects the export potential based on current MLD and light availability, the  
339 biological pump efficiency reflects the potential as derived from nutrient distribution in the oceans,  
340 estimated from the extent of nutrient removal from the surface ocean (Sarmiento and Gruber, 2006)  
341 or the proportion of regenerated nutrients at depth (Ito and Follows, 2005). A revised estimate of  
342 the global biological pump efficiency, estimated based on the proportion of regenerated to total  
343 nutrients (preformed + regenerated) at depth is around 30-35% (Duteil et al., 2013). The  $ef$  ratio  
344 on the other hand describes how much of production is exported as opposed to recycled in the  
345 surface (Dunne et al., 2005). The ultra-oligotrophic subtropical waters have a low export ratio, a  
346 strong biological pump efficiency with exhaustion of nutrients at the ocean surface, and therefore  
347 have not reached their full light potential (low  $f_{pt}$ ) because of the strong stratification and nutrient  
348 limitation. The seasonal pattern of  $f_{pt}$  in the subantarctic region suggests that the low biological  
349 pump efficiency is the result of light limitation in the austral spring and nutrient (likely Fe) and  
350 light limitation in the austral summer.

#### 351 **4. Caveats and limitations**

352 There are a multitude of uncertainties, simplifications, and approximations in our model and  
353 field observations. Among others:

- 354 • In our study, we used a model which builds on Sverdrup's critical depth hypothesis. There  
355 are competing hypotheses to explain phytoplankton bloom phenology (timing and  
356 intensity), including the "dilution recoupling hypothesis" or "disturbance recovery

357 hypothesis” (Behrenfeld, 2010; Boss and Behrenfeld, 2010) and “critical turbulence  
358 hypothesis” (Brody and Lozier, 2015; Huisman et al., 1999; Taylor and Ferrari, 2011). In  
359 the case of top-down control, any respiratory grazing loss not accounted for by our loss  
360 term would behave as a system not reaching its full light potential (NCP\*). Conversely,  
361 any grazing loss associated with export (e.g., rapidly sinking fecal pellets and other  
362 zooplankton-mediated export pathways) would minimize respiratory losses thereby  
363 bringing NCP closer to its upper bound based on light-availability. These opposing effects  
364 are beyond the scope of this study, but could be modeled, especially as we learn more about  
365 their impacts on carbon fluxes through new efforts such as NASA’s EXPORTS program  
366 (Siegel et al., 2016). See also the point below on mixing vs. mixed layer depth.

- 367 • Phytoplankton biomass concentration ( $C$ ) may vary with depth in the mixed layer,  
368 especially for water columns experiencing varying degrees of turbulent mixing. In addition,  
369 MLD is not always the best proxy of light availability with mixing layer in some cases  
370 deviating from the mixed layer (Franks, 2015; Huisman et al., 1999). The factors defining  
371 the MLD also vary in different oceanic regions.
- 372 • For simplicity, we model the dependence of photosynthesis on irradiance assuming  
373 Michaelis-Menten kinetics, which does not account for photoinhibition. More accurate  
374 models can be found in other studies (Platt et al., 1980). Due to optional absorption,  $K_I$   
375 also varies with depth in the mixed layer. Additionally, the linear relationship between  $K_I$   
376 and  $C$  is influenced by CDOM, NAP, and other environmental factors (e.g., solar zenith  
377 angle) (Gordon, 1989).
- 378 •  $\mu_{max}$  and  $r_{HR}$  are influenced by environmental factors other than temperature, including  
379 community structure (Chen and Laws, 2017), and may vary with depth within the mixed

380 layer (Smetacek and Passow, 1990). For these reasons, the equations relating  $\mu_{max}$  and  $r_{HR}$   
381 (i.e.,  $B_t$  and  $P_t$ ) to temperature also carry significant uncertainties (Bissinger et al., 2008;  
382 Edwards et al., 2016; Kremer et al., 2017; López-Urrutia and Morán, 2007; Rivkin and  
383 Legendre, 2001) which impacts our estimates of the upper bound on carbon export,  
384 especially in warmer regions. As in other recent studies (Cael and Follows, 2016; Cael et  
385 al., 2017; Dutkiewicz et al., 2001; Gong et al., 2015; Gong et al., 2017; Huisman et al.,  
386 2006; Taylor and Ferrari, 2011), we model heterotrophic respiration to vary in proportion  
387 to phytoplankton concentration. The model could be further improved by explicitly  
388 including the concentration of heterotrophs. See point above on the grazing effect on export  
389 with regards to  $r_{HR}$ .

- 390 • NCP may underestimate export production when accompanied by a decrease in the  
391 inventory of organic matter in the mixed layer (see introduction and equation (2)).
- 392 • Our field observations are limited, mostly focusing on the spring and summer seasons, and  
393 harbor significant uncertainties. For example, deep mixed layers can bias the  $O_2/Ar$  method  
394 low if entrainment of deeper waters brings low  $O_2$  into the mixed layer. Descriptions of  
395 these uncertainties are presented in other studies (Bender et al., 2011; Cassar et al., 2014;  
396 Jonsson et al., 2013).
- 397 • Finally, our study is only relevant to the mixed layer. It does not account for productivity  
398 below the mixed layer, which can be important in some regions such as the subtropical  
399 ocean.

## 400 **5. Conclusions**

401 In this study, we derived a mechanistic model of an upper bound on carbon export ( $NCP^*$ ) based  
402 on the metabolic balance between photosynthesis and respiration of the plankton community. The

403 upper bound is a positively skewed bell-shaped function of mixed layer depth (MLD). At low  
404 temperatures, the upper bound decreases with temperature if mixed layers are deep, but increases  
405 with temperature if mixed layers are shallow. We used this model to derive a global distribution  
406 of an upper bound on carbon export as a function of MLD and surface PAR, which shows high  
407 values in low latitudes and low values in high latitudes due to deep MLD. To examine how current  
408 export production compares to this upper bound in the world's oceans, we calculated the ratio of  
409 satellite export production estimates to the upper bound derived by our model. High ratios of export  
410 production to *NCP\** in the North Atlantic and ACC indicate that export production in these regions  
411 is likely co-limited by nutrient and light availability. Overall, our results may explain differences  
412 in carbon export measured during past iron fertilization experiments (e.g., subantarctic and polar  
413 regions), inform future iron fertilization experiments, help in the development of remotely-sensed  
414 carbon export algorithms, and improve predictions of the response of marine ecosystems to a  
415 changing climate.

#### 416 **Acknowledgements**

417 We would like to acknowledge NASA GSFC for processing and distributing PAR and SST  
418 products (<http://oceancolor.gsfc.nasa.gov/>). Global Argo temperature-salinity profiling floats were  
419 downloaded from <http://www.usgodae.org/>. CTD casts were downloaded from National  
420 Oceanographic Data Center (<https://www.nodc.noaa.gov/>). N.C. was supported by NSF OPP-  
421 1043339. Z.L. was supported by a NASA Earth and Space Science Fellowship (Grant No.  
422 NNX13AN85H). The authors thank three anonymous reviewers for their insightful comments.

#### 423 **References**

424 Arrigo, K. R., van Dijken, G. L., and Bushinsky, S.: Primary production in the Southern Ocean,  
425 1997-2006, *J. Geophys. Res.*, 113, doi:10.1029/2007JC004551, 2008.

426 Baker, K. S. and Smith, R. C.: Bio-optical classification and model of natural-waters .2, *Limnol.*  
427 *and Oceanogr.*, 27, 500-509, doi:10.4319/lo.1982.27.3.0500, 1982.

428 Behrenfeld, M. J.: Abandoning Sverdrup's Critical Depth Hypothesis on phytoplankton blooms,  
429 *Ecology*, 91, 977–989, doi:10.1890/09-1207.1, 2010.

430 Behrenfeld, M. J. and Falkowski, P. G.: Photosynthetic rates derived from satellite-based  
431 chlorophyll concentration, *Limnol. and Oceanogr.*, 42, 1-20,  
432 doi:10.4319/lo.1997.42.1.0001, 1997.

433 Bender, M. L., Tilbrook, B., Cassar, N., Jonsson, B. F., Poisson, A., and Trull, T. W.: Ocean  
434 productivity south of Australia during spring and summer, *Deep-Sea Res. Pt. I*, 112, 68-78,  
435 doi:10.1016/j.dsr.2016.02.018, 2016.

436 Bender, M. L., Kinter, S., Cassar, N., and Wanninkhof, R.: Evaluating gas transfer velocity  
437 parameterizations using upper ocean radon distributions, *J. Geophys. Res.*, 116,  
438 doi:10.1029/2009JC005805, 2011.

439 Bissinger, J. E., Montagnes, D. J. S., Sharples, J., and Atkinson, D.: Predicting marine  
440 phytoplankton maximum growth rates from temperature: Improving on the Eppley curve  
441 using quantile regression, *Limnol. Oceanogr.*, 53, 487–493,  
442 doi:10.4319/lo.2008.53.2.0487, 2008.

443 Boss, E. and Behrenfeld, M. J.: In situ evaluation of the initiation of the North Atlantic  
444 phytoplankton bloom, *Geophys. Res. Lett.*, 37, doi:10.1029/2010GL044174, 2010.

445 Boyd, P. W., Jickells, T., Law, C. S., Blain, S., Boyle, E. A., Buesseler, K. O., Coale, K. H., Cullen,  
446 J. J., de Baar, H. J. W., Follows, M., Harvey, M., Lancelot, C., Levasseur, M., Owens, N.  
447 P. J., Pollard, R., Rivkin, R. B., Sarmiento, J., Schoemann, V., Smetacek, V., Takeda, S.,  
448 Tsuda, A., Turner, S., and Watson, A. J.: Mesoscale iron enrichment experiments 1993-  
449 2005: Synthesis and future directions, *Science*, 315, 612-617,  
450 doi:10.1126/science.1131669, 2007.

451 Boyd, P. W., Watson, A. J., Law, C. S., Abraham, E. R., Trull, T., Murdoch, R., Bakker, D. C. E.,  
452 Bowie, A. R., Buesseler, K. O., Chang, H., Charette, M., Croot, P., Downing, K., Frew, R.,  
453 Gall, M., Hadfield, M., Hall, J., Harvey, M., Jameson, G., LaRoche, J., Liddicoat, M., Ling,  
454 R., Maldonado, M. T., McKay, R. M., Nodder, S., Pickmere, S., Pridmore, R., Rintoul, S.,  
455 Safi, K., Sutton, P., Strzepek, R., Tanneberger, K., Turner, S., Waite, A., and Zeldis, J.: A

456 mesoscale phytoplankton bloom in the polar Southern Ocean stimulated by iron  
457 fertilization, *Nature*, 407, 695-702, doi:10.1038/35037500, 2000.

458 Britten, G. L., Wakamatsu, L., and Primeau, F. W.: The temperature-ballast hypothesis explains  
459 carbon export efficiency observations in the Southern Ocean, *Geophys. Res. Lett.*, 44,  
460 1831-1838, doi:10.1002/2016GL072378, 2017.

461 Brody, S. R. and Lozier, M. S.: Characterizing upper-ocean mixing and its effect on the spring  
462 phytoplankton bloom with in situ data, *ICES J. Mar. Sci.*, 72, 1961–1970.  
463 doi:10.1093/icesjms/fsv006, 2015

464 Cael B. B., Bisson, K., and Follows, M. J.: How have recent temperature changes affected the  
465 efficiency of ocean biological carbon export? *Limnology and Oceanography Letters*, 2,  
466 113-118, doi:10.1002/lol2.10042, 2017.

467 Cael, B. B. and Follows, M. J.: On the temperature dependence of oceanic export efficiency,  
468 *Geophys. Res. Lett.*, 43, 5170-5175, doi:10.1002/2016GL068877, 2016.

469 Cassar, N., Nevison, C. D., and Manizza, M.: Correcting oceanic O<sub>2</sub>/Ar-net community production  
470 estimates for vertical mixing using N<sub>2</sub>O observations, *Geophys. Res. Lett.*, 41, 8961-8970,  
471 doi:10.1002/2014GL062040, 2014.

472 Cassar, N., DiFiore, P. J., Barnett, B. A., Bender, M. L., Bowie, A. R., Tilbrook, B., Petrou, K.,  
473 Westwood, K. J., Wright, S. W., and Lefevre, D.: The influence of iron and light on net  
474 community production in the Subantarctic and Polar Frontal Zones, *Biogeosciences*, 8,  
475 227-237, doi:10.5194/bg-8-227-2011, 2011.

476 Cassar, N., Wright, S. W., Thomson, P. G., Trull, W. T., Westwood, K. J., de Salas, M., Davidson,  
477 A., Pearce, I., Davies, D. M., and Matear, R. J.: The relation of mixed-layer net community  
478 production to phytoplankton community composition in the Southern Ocean, *Global*  
479 *Biogeochem. Cy.*, 29, 446-462, doi:10.1002/2014GB004936, 2015.

480 Chang, C.-H., Johnson, N. C., and Cassar, N.: Neural network-based estimates of Southern Ocean  
481 net community production from in situ O<sub>2</sub>/Ar and satellite observation: a methodological  
482 study, *Biogeosciences*, 11, 3279-3297, <https://doi.org/10.5194/bg-11-3279-2014>, 2014.

483 Chen, B., Laws, E. A.: Is there a difference of temperature sensitivity between marine  
484 phytoplankton and heterotrophs? *Limnol. and Oceanogr.*, 62, 806-817,  
485 doi:10.1002/lno.10462, 2017.

486 Cullen, J. J. and Lewis, M. R.: The kinetics of algal photoadaptation in the context of vertical  
487 mixing, *J. Plankton Res.*, 10, 1039-1063, doi:10.1093/plankt/10.5.1039, 1988.

488 de Barr, J. W. H., Boyd, P. W., Coale, K. H., Landry M. R., Tsuda, A., Assmy, P., Bakker, D. C.  
489 E., Bozec, Y., Barber, R. T., Brzezinski, M. A., Buesseler, K. O., Boyé, M., Croot, P. L.,  
490 Gervais, F., Gorbunov, M. Y., Harrison, P. J., Hiscock, W. T., Laan, P., Lancelot, C., Law,  
491 C. S., Levasseur, M., Marchetti, A., Millero, F. J., Nishioka, J., Nojiri, Y., van Oijen, T.,  
492 Riebesell, U., Rijkenberg, M. J. A., Saito, H., Takeda, S., Timmermans, K. R., Veldhuis,  
493 M. J. W., Waite, A. M., and Wong, C. S.: Synthesis of iron fertilization experiments: From  
494 the Iron age in the Age of Enlightenment, *J. Geophys. Res.*, 110, C09S16,  
495 doi:10.1029/2004JC002601, 2005.

496 Dunne, J. P., Armstrong, R. A., Gnanadesikan, A., and Sarmiento, J. L.: Empirical and mechanistic  
497 models for the particle export ratio, *Global Biogeochem. Cy.*, 19,  
498 doi:10.1029/2004GB002390, 2005.

499 Duteil, O., Koeve, W., Oschlies, A., Bianchi, D., Galbraith, E., Kriest, I., and Matar, R.: A novel  
500 estimate of ocean oxygen utilisation points to a reduced rate of respiration in the ocean  
501 interior, *Biogeosciences*, 10, 7723-7738, <https://doi.org/10.5194/bg-10-7723-2013>, 2013.

502 Dutkiewicz, S., Follows, M., Marshall, J., and Gregg, W. W.: Interannual variability of  
503 phytoplankton abundances in the North Atlantic, *Deep-Sea Res. Pt. II*, 48, 2323-2344,  
504 doi:10.1016/S0967-0645(00)00178-8, 2001.

505 Edwards, K. F., Thomas, M. K., Klausmeier, C. A., and Litchman, E.: Phytoplankton growth and  
506 the interaction of light and temperature: A synthesis at the species and community  
507 level, *Limnol. and Oceanogr.*, 61, 1232–1244, doi:10.1002/lno.10282, 2016.

508 Eppley, R. W.: Temperature and phytoplankton growth in the sea, *Fishery Bulletin*, 70, 1063-1085,  
509 1972.

510 Eveleth, R., Cassar, N., Sherrell, R. M., Ducklow, H., Meredith, M., Venables, H., Lin, Y., and Li,  
511 Z.: Ice melt influence on summertime net community production along the Western  
512 Antarctic Peninsula, *Deep-Sea Res. Pr. II*, 139, 89-102, doi:10.1016/j.dsr2.2016.07.016,  
513 2017.

514 Falkowski, P. G., Barber, R. T., and Smetacek, V.: Biogeochemical controls and feedbacks on  
515 ocean primary production, *Science*, 281, 200-206, doi:10.1126/science.281.5374.200,  
516 1998.

517 Franks, P. J. S.: Has Sverdrup's critical depth hypothesis been tested? Mixed layers vs. turbulent  
518 layers, *ICES J. Mar. Sci.*, 72, 1897-1907, doi:10.1093/icesjms/fsu175, 2015.

519 Gong, X., Shi, J., Gao, H. W., and Yao, X. H.: Steady-state solutions for subsurface chlorophyll  
520 maximum in stratified water columns with a bell-shaped vertical profile of chlorophyll,  
521 *Biogeosciences*, 12, 905-919, doi:10.5194/bg-12-905-2015, 2015.

522 Gong, X., Jiang, W., Wang, L., Gao, H., Boss, E., Yao, X., Kao, S., and Shi, J.: Analytical solution  
523 of the nitracline with the evolution of subsurface chlorophyll maximum in stratified water  
524 columns, *Biogeosciences*, 14, 2371-2386, doi:10.5194/bg-14-2371-2017, 2017.

525 Gordon, H. R.: Can the Lambert-Beer law be applied to the diffuse attenuation coefficient of ocean  
526 water, *Limnol. and Oceanogr.*, 34, 1389-1409, doi:10.4319/lo.1989.34.8.1389, 1989.

527 Henson, S. A., Yool, A., and Sanders, R.: Variability in efficiency of particulate organic carbon  
528 export: A model study, *Global Biogeochem. Cy.*, 29, 33-45, doi:10.1002/2014GB004965,  
529 2015.

530 Henson, S. A., Sanders, R., Madsen, E., Morris, P. J., Le Moigne, F., and Quartly, G. D.: A reduced  
531 estimate of the strength of the ocean's biological carbon pump, *Geophys. Res. Lett.*, 38,  
532 L04606, doi:10.1029/2011GL046735, 2011.

533 Huang, K., Ducklow, H., Vernet, M., Cassar, N., and Bender, M. L.: Export production and its  
534 regulating factors in the West Antarctica Peninsula region of the Southern Ocean, *Global*  
535 *Biogeochem. Cy.*, 26, GB2005, doi:10.1029/2010GB004028, 2012.

536 Huisman, J. and Weissing, F. J.: Light-limited growth and competition for light in well-mixed  
537 aquatic environments: An elementary model, *Ecology*, 75, 507-520, doi:10.2307/1939554,  
538 1994.

539 Huisman, J., van Oostveen, P., and Weissing, F. J.: Critical depth and critical turbulence: Two  
540 different mechanisms for the development of phytoplankton blooms, *Limnol. and*  
541 *Oceanogr.*, 44, 1781-1787, doi:10.4319/lo.1999.44.7.1781, 1999.

542 Huisman, J., Thi, N. N. P., Karl, D. M., and Sommeijer B.: Reduced mixing generates oscillations  
543 and chaos in the oceanic deep chlorophyll maximum, *Nature*, 439, 322-325,  
544 doi:10.1038/nature04245, 2006.

545 Ito, T., and Follows, M. J.: Preformed phosphate, soft tissue pump and atmospheric CO<sub>2</sub>, *J. Mar.*  
546 *Res.*, 63, 813-839, doi:10.1357/0022240054663231, 2005.



547 Jonsson, B. F., Doney, S. C., Dunne, J., and Bender, M.: Evaluation of the Southern Ocean O<sub>2</sub>/Ar-  
548 based NCP estimates in a model framework, *J. Geophys. Res.*, 118, 385-399,  
549 doi:10.1002/jgrg.20032, 2013.

550 Kremer, C. T., Thomas, M. K., and Litchman, E.: Temperature- and size-scaling of phytoplankton  
551 population growth rates: Reconciling the Eppley curve and the metabolic theory of ecology,  
552 *Limnol. and Oceanogr.*, 62, 1658-1670, doi:10.1002/lno.10523, 2017.

553 Laws, E. A., Falkowski, P. G., Smith, W. O., Ducklow, H., and McCarthy, J. J.: Temperature  
554 effects on export production in the open ocean, *Global Biogeochem. Cy.*, 14, 1231-1246,  
555 doi:10.1029/1999GB001229, 2000.

556 Lewis, M. R., Cullen, J. J., and Platt, T.: Relationships between vertical mixing and  
557 photoadaptation of phytoplankton: Similarity criteria, *Mar. Ecol. Prog. Ser.*, 15, 141-149,  
558 doi:10.3354/meps015141, 1984.

559 Li, Z. and Cassar, N.: Satellite estimates of net community production based on O<sub>2</sub>/Ar observations  
560 and comparison to other estimates, *Global Biogeochem. Cy.*, 30, 735-752,  
561 doi:10.1002/2015GB005314, 2016.

562 Li, Z., Cassar, N., Huang, K., Ducklow, H., and Schofield, O.: Interannual variability in net  
563 community production at the Western Antarctic Peninsula region (1997-2014), *J. Geophys.*  
564 *Res.*, 121, 4748-4762, doi:10.1002/2015JC011378, 2016.

565 López-Urrutia, A. and Morán, X. A. G.: Resource limitation of bacterial production distorts the  
566 temperature dependence of oceanic carbon cycling, *Ecology*, 88, 817-822,  
567 doi:10.1890/06-1641, 2007.

568 López-Urrutia, Á., San Martín, E., Harris, R. P., and Irigoien, X.: Scaling the metabolic balance  
569 of the oceans, *Proc. Natl Acad. Sci. USA*, 103, 8739-8744, doi:10.1073/pnas.0601137103,  
570 2006.

571 Maiti, K., Charette, M. A., Buesseler, K. O., and Kahru M.: An inverse relationship between  
572 production and export efficiency in the Southern Ocean, *Geophys. Res. Lett.*, 40, 1557-  
573 1561, doi:10.1002/grl.50219, 2013.

574 Martin, J. H., Knauer, G. A., Karl, D. M., and Broenkow, W. W.: VERTEX: carbon cycling in the  
575 northeast Pacific, *Deep-Sea Res. Pr. A*, 34, 267-285, doi:10.1016/0198-0149(87)90086-0,  
576 1987.

577 Martin, P., Rutgers van der Loeff, M., Cassar, N., Vandromme, P., d'Ovidio, F., Stemman, L.,  
578 Rengarajan, R., Soares, M., Gonzalez, H. E., Ebersbach, F., Lampitt, R., Sanders, R.,  
579 Barnett, B., Smetacek, V., and Naqvi, S. W. A.: Iron fertilization enhanced net community  
580 production but not downward particle flux during the Southern Ocean iron fertilization  
581 experiment LOHAFEX, *Global Biogeochem. Cy.*, 27, 871–881, doi:10.1002/gbc.20077,  
582 2013.

583 Mitchell, B. G. and Holm-Hansen, O.: Observations and modeling of the Antarctic phytoplankton  
584 crop in relation to mixing depth, *Deep-Sea Res. Pr. A*, 38, 981-1007, doi:10.1016/0198-  
585 0149(91)90093-U, 1991.

586 Mitchell, B. G., Brody, E. A., Holm-Hansen, O., McClain, C., and Bishop, J.: Light limitation of  
587 phytoplankton biomass and macronutrient utilization in the Southern Ocean, *Limnol. and*  
588 *Oceanogr.*, 36, 1662-1677, doi:10.4319/lo.1991.36.8.1662, 1991.

589 Morel, A. and Prieur, L.: Analysis of variations in ocean color, *Limnol. and Oceanogr.*, 22, 709-  
590 722, doi:10.4319/lo.1977.22.4.0709, 1977.

591 Mouw, C. B., Barnett, A., McKinley, G., Gloege, L., and Pilcher, D.: Global ocean particulate  
592 organic carbon flux merged with satellite parameters, *Earth Syst. Sci. Data*, 8, 531-541,  
593 doi:10.5194/essd-8-531-2016, 2016.

594 Nelson, D. M. and Smith, W. O.: Sverdrup revisited: Critical depths, maximum chlorophyll levels,  
595 and the control of Southern Ocean productivity by the irradiance-mixing regime, *Limnol.*  
596 *and Oceanogr.*, 36, 1650-1661, doi:10.4319/lo.1991.36.8.1650, 1991.

597 Platt, T., Gallegos, C. L., and Harrison, W. G.: Photoinhibition of photosynthesis in natural  
598 assemblages of marine phytoplankton, *J. Mar. Res.*, 38, 687-701, 1980.

599 Rivkin, R. B. and Legendre, L.: Biogenic carbon cycling in the upper ocean: Effects of microbial  
600 respiration, *Science*, 291, 2398-2400, doi:10.1126/science.291.5512.2398, 2001.

601 Sarmiento, J. L. and Gruber, N.: *Ocean Biogeochemical Dynamics*, Princeton University Press,  
602 Princeton, New Jersey, 2006.

603 Shadwick, E. H., Tilbrook, B., Cassar, N., Trull, T. W., and Rintoul, S. R.: Summertime physical  
604 and biological controls on O<sub>2</sub> and CO<sub>2</sub> in the Australian Sector of the Southern Ocean, *J.*  
605 *Marine Syst.*, 147, 21-28, doi:10.1016/j.jmarsys.2013.12.008, 2015.

606 Siegel, D. A., Buesseler, K. O., Behrenfeld, M. J., Benitez-Nelson, C. R., Boss, E., Brzezinski, M.  
607 A., Burd, A., Carlson, C. A., D'Asaro, E. A., Doney, S. C., Perry, M. J., Stanley, R. H. R.,

608 and Steinberg, D. K.: Prediction of the export and fate of global ocean net primary  
609 production: The exports science plan, *Front. Mar. Sci.*, 3, doi:10.3389/fmars.2016.00022,  
610 2016.

611 Sigman, D. M. and Boyle, E. A.: Glacial/interglacial variations in atmospheric carbon dioxide,  
612 *Nature*, 407, 859-869, doi:10.1038/35038000, 2000.

613 Smetacek, V. and Passow, U.: Spring bloom initiation and Sverdrup's critical depth model, *Limnol.*  
614 *and Oceanogr.*, 35, 228–234, doi:10.4319/lo.1990.35.1.0228, 1990.

615 Smith, R. C. and Baker, K. S.: Optical classification of natural waters, *Limnol. and Oceanogr.*, 23,  
616 260-267, doi:10.4319/lo.1978.23.2.0260, 1978a.

617 Smith, R. C. and Baker, K. S.: The bio-optical state of ocean waters and remote sensing, *Limnol.*  
618 *and Oceanogr.*, 23, 247-259, doi:10.4319/lo.1978.23.2.0247, 1978b.

619 Stange, P., Bach, L. T., Le Moigne, F. A. C., Taucher, J., Boxhammer, T., and Riebesell, U.:  
620 Quantifying the time lag between organic matter production and export in the surface ocean:  
621 Implications for estimates of export efficiency, *Geophys. Res. Lett.*, 44, 268-276,  
622 doi:10.1002/2016GL07087, 2017.

623 Sunda, W. G. and Huntsman, S. A.: Interrelated influence of iron, light and cell size on marine  
624 phytoplankton growth, *Nature*, 390, 389-392, doi:10.1038/37093, 1997.

625 Sverdrup, H. U., On conditions for the vernal blooming of phytoplankton, *Journal du Conseil*  
626 *International pour l'Exploration de la Mer*, 18, 287-295, doi:10.1093/icesjms/18.3.287,  
627 1953.

628 Taylor, J. R. and Ferrari, R.: Shutdown of turbulent convection as a new criterion for the onset of  
629 spring phytoplankton blooms, *Limnol. And Oceanogr.*, 56, 2293-  
630 2307, doi:10.4319/lo.2011.56.6.2293, 2011.

631 Tortell, P. D., Bittig, H. C., Körtzinger, A., Jones, E. M., and Hoppema, M.: Biological and  
632 physical controls on N<sub>2</sub>, O<sub>2</sub>, and CO<sub>2</sub> distributions in contrasting Southern Ocean surface  
633 waters, *Global Biogeochem. Cy.*, 29, 994-1013, doi:10.1002/2014GB004975, 2015.

634 Volk, T. and Hoffert, M. I.: Ocean carbon pumps: Analysis of relative strengths and efficiencies  
635 in ocean-driven atmospheric CO<sub>2</sub> changes, in: *The Carbon Cycle and Atmospheric CO<sub>2</sub>:  
636 Natural Variations Archean to Present*, *Geophys. Monogr. Ser.*, Vol. 32, edited by  
637 Sundquist, E. T. and Broecker, W. S., AGU, Washington, D. C., 99-110, 1985.

638 Werdell, P. J. and Bailey, S. W.: An improved in-situ bio-optical data set for ocean color algorithm  
639 development and satellite data product validation, *Remote Sensing of Environment*, 98,  
640 122-140, doi:10.1016/j.rse.2005.07.001, 2005.

641 White, P. A., Kalff, J., Rasmussen, J. B., and Gasol, J. M.: The effect of temperature and algal  
642 biomass on bacterial production and specific growth rate in fresh water and marine habitats,  
643 *Microb. Ecol.*, 21, 99-118, 1991.

644

645

646 **Table 1.** Model symbols, abbreviations, and units

Symbol	Description	Units
MLD	Mixed layer depth	m
$MLD_{C^*_{max}}$	Maximum MLD corresponds to maximum achievable autotroph's biomass concentration	m
$z$	Depth	m
$Z_c$	Critical depth	m
$Z_p$	Compensation depth	m
$GPP(0,z)$	Gross primary production	$\text{mmol C m}^{-2} \text{d}^{-1}$
$NPP(z)$	Net primary production at depth $z$	$\text{mmol C m}^{-3} \text{d}^{-1}$
$NPP(0,z)$	Net primary production above depth $z$	$\text{mmol C m}^{-2} \text{d}^{-1}$
$NCP(z)$	Net community production at depth $z$	$\text{mmol C m}^{-3} \text{d}^{-1}$
$NCP(0,z)$	Net community production above depth $z$	$\text{mmol C m}^{-2} \text{d}^{-1}$
$HR(z)$	Heterotrophic respiration at depth $z$	$\text{mmol C m}^{-3} \text{d}^{-1}$
$HR(0,z)$	Heterotrophic respiration above depth $z$	$\text{mmol C m}^{-2} \text{d}^{-1}$
$NCP^*$	The maximum NCP for a given MLD (upper bound on carbon export)	$\text{mmol C m}^{-2} \text{d}^{-1}$
$NCP_B$	NCP normalized to autotroph's biomass inventory in the mixed layer	$\text{d}^{-1}$
$ef$	Export ratio	unitless
$f_{pt}$	Ratio of satellite export production estimates to the upper bound on carbon export	unitless
$N$	Nutrient concentration	$\text{mmol m}^{-3}$
$k_m^N$	Half-saturation constant for nutrient concentration	$\text{mmol m}^{-3}$
$N_m$	Nutrient effect on phytoplankton grow $N_m = \frac{N}{N+k_m^N}$	unitless
PAR	Photosynthetically active radiation	$\text{Einstein m}^{-2} \text{d}^{-1}$
$I_0$	Photosynthetically active radiation just beneath water surface	$\text{Einstein m}^{-2} \text{d}^{-1}$
$I(z)$	Photosynthetically active radiation at depth $z$	$\text{Einstein m}^{-2} \text{d}^{-1}$
$k_m^I$	Half-saturation constant for irradiance	$\text{Einstein m}^{-2} \text{d}^{-1}$
$I_m(z)$	Light effect on phytoplankton grow at depth $z$ , $I_m(z) = \frac{I(z)}{I(z)+k_m^I} = \frac{I_0 \times e^{-K_I \times z}}{I_0 \times e^{-K_I \times z} + k_m^I}$	unitless
$I_m(0, z)$	Integrated light effect on phytoplankton grow above depth $z$ , $I_m(0, z) = -\frac{1}{K_I} \times \ln\left(\frac{I_0 \times e^{-K_I \times z} + k_m^I}{I_0 + k_m^I}\right)$	unitless
$PAR_{ML}$	Average PAR in the mixed layer ( $PAR_{ML} = \frac{1-e^{-K_I \times MLD}}{K_I \times MLD} \times I_0$ )	$\text{Einstein m}^{-2} \text{d}^{-1}$
$\mu$	Phytoplankton growth rate	$\text{d}^{-1}$
$\mu_{max}$	Maximum phytoplankton growth rate	$\text{d}^{-1}$

$\mu_{max}^0$	Maximum phytoplankton growth rate for $T = 0$ °C	$d^{-1}$
$r_{HR}$	Heterotrophic respiration ratio	$d^{-1}$
$r_{HR}^0$	Heterotrophic respiration ratio for $T = 0$ °C	$d^{-1}$
$K_I$	Light attenuation coefficient ( $K_I = K_I^w + K_I^{nw}$ )	$m^{-1}$
$K_I^w$	Light attenuation coefficient due to water	$m^{-1}$
$K_I^{nw}$	Light attenuation coefficient due to optically active components	$m^{-1}$
$k_c$	Specific attenuation coefficient for irradiance	$m^2 \text{ mmol}^{-1}$
$C$	Phytoplankton biomass concentration	$\text{mmol m}^{-3}$
$C^*$	Phytoplankton biomass concentration that maximizes NCP	$\text{mmol m}^{-3}$
$C_{max}^*$	Maximum achievable autotroph's biomass concentration	$\text{mmol m}^{-3}$
POC	Particulate organic carbon	$\text{mmol m}^{-3}$
DOC	Dissolved organic carbon	$\text{mmol m}^{-3}$
CDOM	Colored dissolved organic matter	$m^{-1}$
NAP	Non-algal particles	$\text{mmol m}^{-3}$
$T$	Temperature	°C
$P_t$	Temperature dependence for phytoplankton grow rate	°C <sup>-1</sup>
$B_t$	Temperature dependence for heterotrophic respiration ratio	°C <sup>-1</sup>
CO <sub>2</sub>	Carbon dioxide	ppmv

647

648

649 **Table 2.** Value or range of values with references for the parameters used in the model.  
 650

Parameter	Range or value	Reference
$K_I^w$	0.09	(Werdell and Bailey, 2005)
$k_c$	0.03	(Werdell and Bailey, 2005)
Carbon to chlorophyll ratio	90	(Arrigo et al., 2008)
$k_m^I$	4.1 Einstein $m^{-2} d^{-1}$	(Behrenfeld and Falkowski, 1997)
$P_t$	0.0663	(Eppley, 1972)
$B_t$	0.08	(Rivkin and Legendre, 2001; López-Urrutia et al., 2006)
$\mu_{max}$	1 $d^{-1}$ , 1.2 $d^{-1}$	(Laws et al., 2000; Eppley, 1972)
$r_{HR}$	0.1 $d^{-1}$ , 0.2 $d^{-1}$	(Laws et al., 2000; Mitchell et al., 1991)

651

652

653

654 **Figure 1.** Schematic diagram of depth-profiles of net community production (NCP), net primary  
655 production (NPP), and heterotrophic respiration (HR). Yellow and black dots represent the  
656 compensation and critical depths, respectively.

657  
658 **Figure 2.** Relationship between net primary production (NPP), heterotrophic respiration (HR),  
659 net community production (NCP), and phytoplankton biomass concentration (C) for a given  
660 mixed layer depth (MLD). Hatched area in panel A represents NCP. The yellow dot represents  
661 the maximal NCP (NCP\*) obtainable for a given MLD, with the corresponding phytoplankton  
662 biomass concentration (C\*) denoted with a cyan dot. NCP on the right of the yellow dot  
663 decreases with C due to self-shading. Black dot represents depth-integrated NCP = 0 (i.e.,  
664 NPP=HR), with the corresponding phytoplankton biomass concentration defined as critical  
665 biomass (C<sub>c</sub>) and denoted with a blue dot. Ecosystems on the left and right of this threshold are  
666 net autotrophic and heterotrophic, respectively. The asymptote (dashed blue line) in panel B  
667 represents a system dominated by heterotrophic respiration (i.e., NCP ≈ HR >> NPP).

668  
669 **Figure 3.** Upper bounds derived using the original and approximated models. The upper bound  
670 for the original model (equations (8-10)) is estimated through a non-linear optimization  
671 approach. The upper bound for the approximated model is calculated analytically from equation  
672 (19). The models use the constants listed in Table 2 and  $I_m(0) = 0.9$ . Decreasing  $I_m(0)$  and  
673 increasing  $r_{HR}$  results in greater discrepancies between the original and approximated models in  
674 regions with shallow mixed layers.

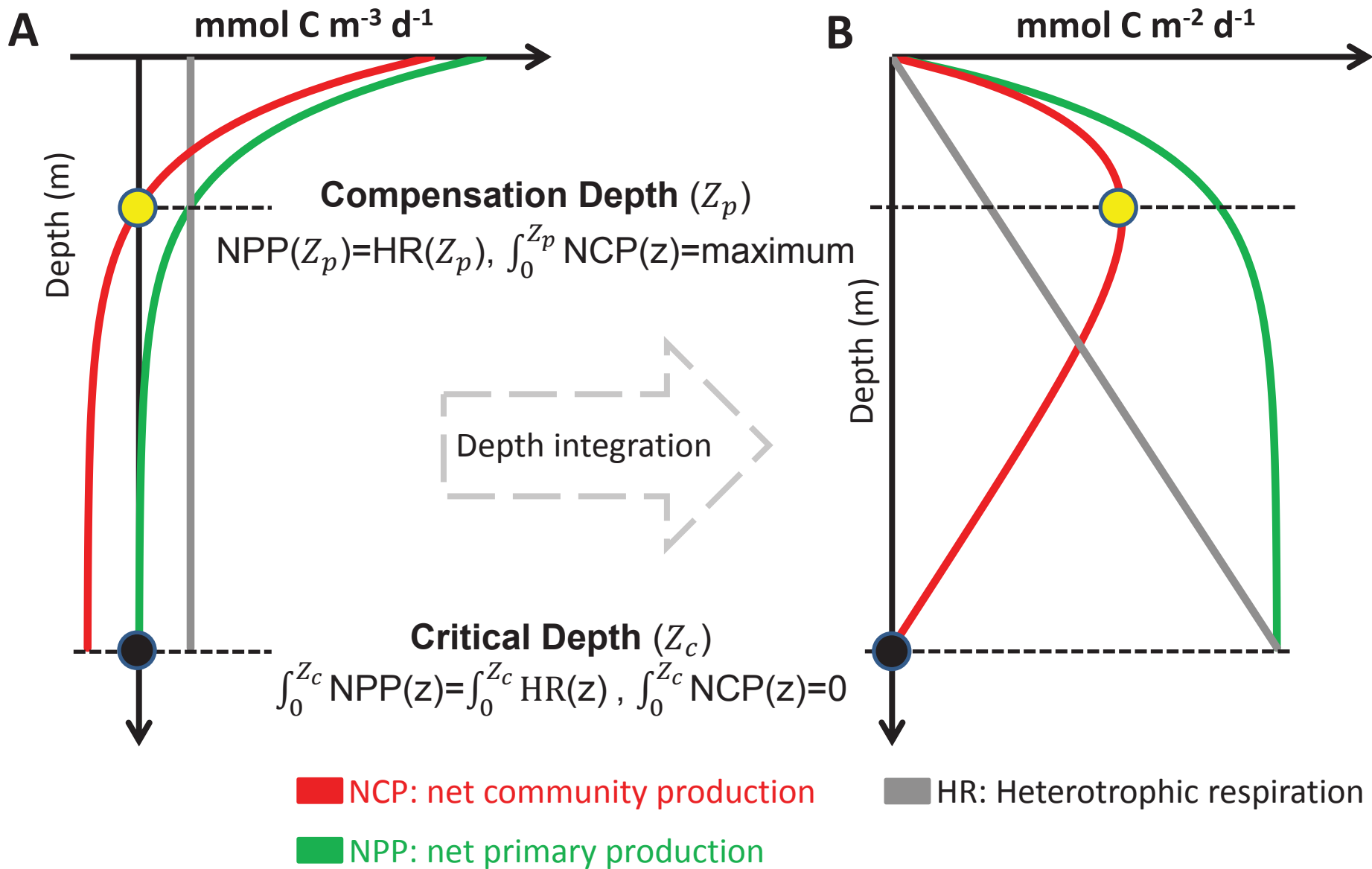
675  
676 **Figure 4.** Modeled upper bound on carbon export production compared to field observations as a  
677 function of mixed layer depth (MLD) and sea surface temperature (SST). (A) The thick gray line  
678 represents the upper bound fitted to the net community production (NCP) data. Dash-lines

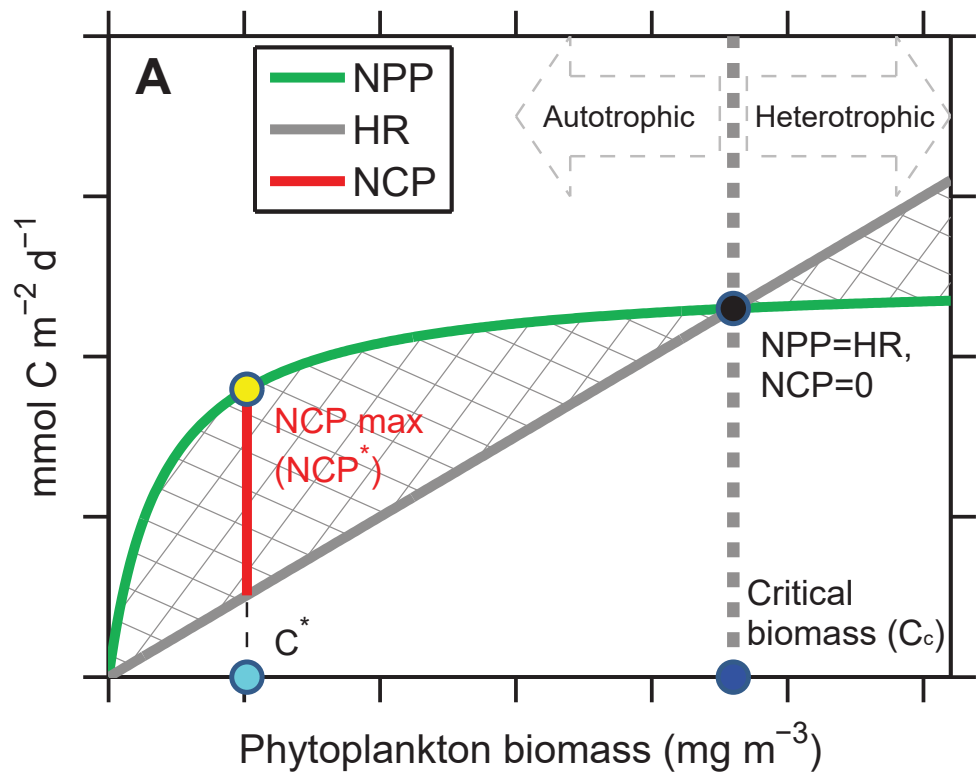


679 represent the upper bounds calculated using parameters available in the literature (Table 2). (B)  
680 NCP as a function of SST with isopleths of constant upper bounds color coded for MLD. NCP  
681 observations are color coded with MLD. (C) Surface representing the envelope of the modeled  
682 upper bound of carbon export production as a function of SST and MLD. Bars represent field  
683 observations color coded with the ratio of NCP to the upper bound. Observations are based on  
684  $^{234}\text{Th}$  and sediment traps estimates of carbon export production and  $\text{O}_2/\text{Ar}$ -derived NCP. A  
685 stoichiometric ratio of  $\text{O}_2/\text{C}=1.4$  was used to convert NCP from  $\text{O}_2$  to C units (Laws, 1991). To  
686 account for the effect of PAR on export production, both MLD and carbon fluxes are normalized  
687 to  $-\log(1 - I_m(0))$  (see equations (19) and (21)). The temperature dependence of  $r_{HR}$  was  
688 modeled as  $r_{HR} = r_{HR}^0 \times e^{0.08 \times T}$ .

689  
690 **Figure 5.** (A) Modeled upper bound on carbon export derived from equation (19), (B-D) ratios  
691 of satellite export production estimates to the upper bound on carbon export, (E) biological pump  
692 efficiency calculated as the difference in nutrient concentrations between surface and depth,  
693 normalized to nutrient concentrations at depth (Sarmiento and Gruber, 2006) (nitrate  
694 concentration from World Ocean Atlas (<https://www.nodc.noaa.gov/OC5/woa13/>)), and (F)  
695 export ratio derived from Dunne et al. (2005). Annual represents annually-integrated value.  
696 Spring and summer represent average value in spring and summer, respectively. In the northern  
697 hemisphere, spring and summer seasons are defined as March-May and June-August,  
698 respectively. In the southern hemisphere, spring and summer seasons are defined as September-  
699 November and December-February, respectively.

700





$NCP = NPP - HR$

